

Preparation of a Novel Active Fischer–Tropsch Co–Ni Catalyst Derived from Metal–Organic Framework

H. Janani^{a, *}, A. Rezvani^{a, **}, and A. A. Mirzaei^{a, ***}

^a*Department of Chemistry, Faculty of Science, University of Sistan and Baluchestan, Zahedan, 98135-674 Iran*

**e-mail: halimehjanani@yahoo.com*

***e-mail: rezvani2001ir@yahoo.ca*

****e-mail: mirzaei@hamoon.usb.ac.ir*

Received April 10, 2019; revised April 24, 2020; accepted May 12, 2020

Abstract—In the present study, a typical metal–organic framework has been employed for preparation of a novel active Fischer–Tropsch Co–Ni catalyst. Co–Ni catalyst was prepared by glycine–MOF combustion method and was heated in a tube furnace ($2^{\circ}\text{C min}^{-1}$) under air at 750°C for 6 h. Scanning electron micrograph of metal–organic framework shows regularly cubic shaped crystals and they were being deformed into a low density, loose and porous material after it was calcined in the tube furnace. BET surface area and pore volume are $276\text{ m}^2/\text{g}$ and $0.31\text{ cm}^3/\text{g}$ respectively. This active catalyst showed selectivity for long-chain hydrocarbons (C_5^+) of $\sim 52\%$ and for short-chain hydrocarbons ($\text{C}_2\text{--C}_4$) 30%. The relatively high activity (TOF of 2.08 s^{-1} at 340°C) was ascribed to its high porous structure and large pore size of the catalyst which facilitated the diffusion of hydrocarbons. The unique features of this catalyst, including structural tailor ability such as high surface area, porosity, homogeneity and stability enable it to be an active Fischer–Tropsch catalyst.

Keywords: metal–organic framework, glycine–MOF combustion method, Fischer–Tropsch synthesis, Co–Ni catalyst

DOI: 10.1134/S0965544120090121

INTRODUCTION

Metal–organic frameworks (MOFs) are an important class of materials composed of metal ions and organic ligands. They can be converted to porous networks via different methods such as hydrolysis, pyrolysis, hydrothermal or solvothermal crystallization, etc. Design and manufacturing of MOFs has attracted great attention in recent years because of their unique structures and functional properties [1–3]. These organic–inorganic hybrid materials are widely used in gas storage, enantioselective separation, sensor technology, optical application, drug delivery, catalysis, etc. [1–4]. In particular, catalysis is one of the most recently promising applications for MOFs. These materials are able to catalyze a large number of chemical reactions with high efficiency. MOFs-derived materials exhibit high porosity, great surface area, high pore volume and well dispersed metal particle, which are suitable for the catalytic process performance.

Fischer–Tropsch synthesis (FTS) is a well-recognized catalytic process for the conversion of synthesis gas into high quality diesel fuel; the reaction yields a mixture of hydrocarbons of different molecular weights [5, 6]. The common FTS catalysts are based

on Fe, Ni, Co, Ru or Rh as the active metal, with Fe and Co being practical choices. Among them, Co-based catalysts have the features of affordable price, high activity, lower CO_2 emission, and lower water gas shift activity which are the most widely used catalysts for commercial FTS process. The synthesis of bimetallic catalysts containing two or more metallic or oxide phases from metal–organic framework is a novel approach that represent several advantages, such as the superior metal interactions, the homogeneous dispersion of the metal phases, and maximum loading amount, which all conclude to development of ideal catalysts for FT synthesis [7, 8]. Recently, Fe and Co-based catalysts derived from MOFs show high CO conversion, superior selectivity and stable operation. The obtained MOFs derived catalysts exhibited highly dispersed metal phase confined within a porous matrix and high FT activity. These MOFs derived catalysts have been prepared by pyrolysis, hydrolysis, and solvothermal methods [9, 10].

In the present work, we report the utilization of a binuclear metal–organic complex for preparation of an active FT catalyst. Such a metal–organic framework is favorable for manufacture of FT catalyst. Herein, we

demonstrate an approach for preparation of active and stable FTS catalyst using combustion synthetic method of glycine–MOF process. This preparation procedure is derived from the glycine–nitrate combustion method [11] and demonstrates an alternative method for the design of new active FT catalysts. No type of promoter or support has been used in the preparation of this catalyst. Usually supported catalyst are more mechanically stable and have better catalytic activity. However, the strong interaction between metal and support can have a negative effect on catalytic efficiency. Based on the nature of the interaction between metal and support, supported catalysts exhibit significant different catalytic and adsorptive properties. Metal–support interactions affect the catalyst activity and product distribution [12].

Therefore, in order to eliminate the effects of metal–support interactions on catalytic performance, we prepared and utilized un-supported catalyst for FTS. By using this strategy, highly loaded and dispersed cobalt catalyst was synthesized and tested for Fischer–Tropsch synthesis. This catalyst displayed notable CO conversion (75%) and good selectivity towards long-chained hydrocarbons. This MOF-derived catalyst is one of the few cases that, although no additional promoter or support was used for its preparation, it has a good catalytic efficiency in FTS compared to other MOF-derived cobalt catalysts [1–4, 10]. This work would open up a new way to design new Fischer–Tropsch catalysts with a good activity and preferable selectivity by using the appropriate preparation strategy and befitting MOF precursors.

EXPERIMENTAL

Preparation procedure. Metal–organic complex was prepared according to the literature [13]. Addition of (2-methyl-2,4-bis(6-iminopyridin-2-yl)-1H-1,5-benzodiazepine) to equimolar of cobalt (II) dichloride in the mixture of dichloromethane/ethanol generated mononuclear Co complex. Obtained complex reacted with nickel (II) dichloride in ethanol to get the Co–Ni heteronuclear complex. Yellow microcrystals were obtained in good yields (75%). Elemental analysis, FT-IR and UV-vis spectra of the MOF were in agreement with what was reported in the reference. The purity of the sample was confirmed by single crystal X-ray diffraction. FT-IR (KBr, cm^{-1}): 3361, 1620 cm^{-1} ($\nu_{\text{C=N}}$), 1590, 1470, 1369, 1200, 808.1, and 769.1 cm^{-1} .

Then, this MOF precursor was used for the synthesis of FT catalyst. In this strategy, 0.01 mol of metal organic complex and 0.04 mol glycine were added into distilled water. This mixture was stirred by magnetic mixer at 60–70°C until the homogenous sol-like solution was obtained. Then this solution was calcined in a tube furnace at 750°C for 6 h with a heating rate of 2° min^{-1} . Afterwards, the sample was reduced under

H_2 flow (60 mL min^{-1}) at 400°C for 10 h before being tested on the reaction line for FT synthesis.

Catalytic reaction. The Co–Ni catalyst was tested in the FTS in a tubular stainless steel micro-fixed bed reactor at 1 MPa pressure. 1 g of catalyst was reduced in H_2 gas (total flow of 60 mL min^{-1}) at atmospheric pressure and 400°C for 10 h. Hydrogen flow was then stopped and temperature was decreased down to 200°C. At this temperature, the pressure was increased to 1.0 MPa. The catalytic tests were carried out between 260–340°C, 10 h for each temperature at the steady state, syngas with a volume ratio of $\text{H}_2/\text{CO}=2$ (gas mixture containing 32% CO, 63% H_2 , 5% N_2) and gas hourly space velocity (GHSV) of 3600 h^{-1} . The reaction was started by raising the temperature to the desired reaction temperature. The reaction products were analyzed *on-line* by gas chromatograph equipped with a 10-port sampling valve (Supelco company, USA, Visi Model), a sample loop, a thermal conductivity detector, a packed column (Hayesep DB, Alltech Company, USA) and an FID. The selectivity of final products was computed on a carbon basis (Fig. S1).

Instrumentation. Thermogravimetric behavior of the MOF was recorded under air using the BAHRTA 503 (Germany) thermal analyzer from room temperature to 800°C (heating rate of 3° min^{-1}). Electronic spectra, using a JASCO 7850 spectrophotometer. FT-IR spectrum was recorded using a Perkin Elmer FT-IR spectrometer with KBr pellets (Fig. S2). Powder X-ray diffraction (PXRD) measurement were performed on an Inel Equinox 3000 X-Ray Diffractometer using CuK_α radiation. The BET surface areas were measured on a micro metrics adsorption equipment (Quantachrome Instrument, model Nova 2000, USA) determining nitrogen (99.99% purity) as the analysis gas and the samples were slowly heated to 300°C for 6 h under nitrogen atmospheric at –196°C. The scanning electron microscope (SEM) image, electron microprobe analysis (EPMA) and energy dispersive X-ray spectrometer (EDS) were obtained on Philips XL30 scanning electron microscopy (Netherlands). The elemental analysis in the catalyst was measured by atomic adsorption spectroscopy (AAAnalyst 200, Perkin Elmer, USA) and ICP-MS (PerkinElmer's NexION 2000 ICP Mass Spectrometer).

RESULTS AND DISCUSSION

MOF characterization. The crystal structure of this MOF consists of one nickel(II) cation, one cobalt(II) cation, one ligand molecule (2-methyl-2,4-bis(6-iminopyridin-2-yl)-1H-1,5-benzodiazepine), one ethanol molecule and four chlorides. The bis-chelate ligand bridges between cobalt and nickel. The cobalt center adopts distorted trigonal pyramid. The equatorial position is occupied by the nitrogen (N5) of pyridine and the two chlorides. Other two nitrogen atoms

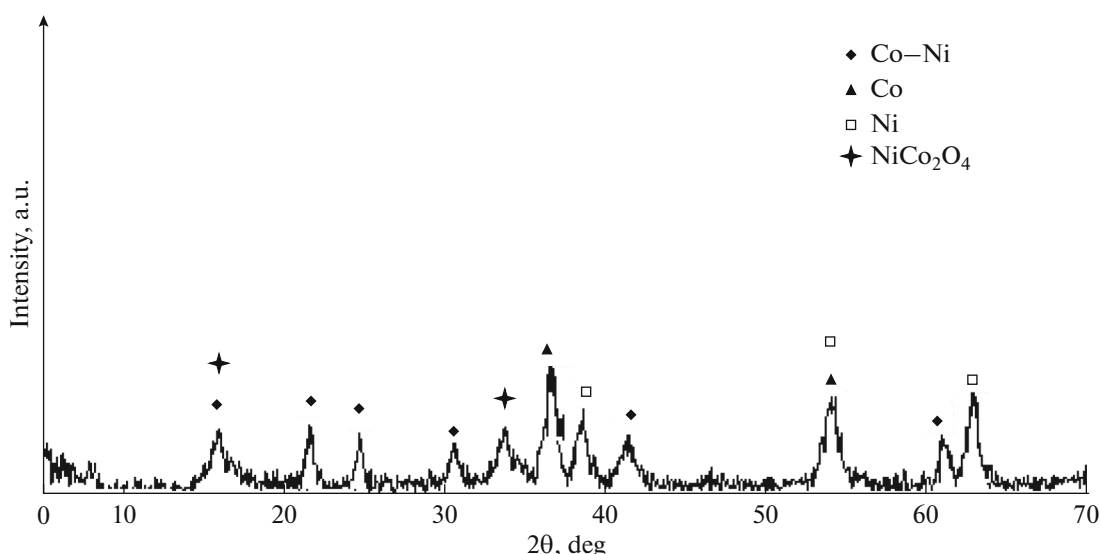


Fig. 1. PXRD pattern of the catalyst.

(N4, N6) are in the axial plane. The coordination geometry at nickel center is distorted octahedron. The FT-IR and elemental analysis were consistent with the literature [13]. The purity of the sample was confirmed by the powder X-ray diffraction. The TGA curve of metal organic framework shows that the first weight lost occurred before 150°C was attributed to the evaporation of ethanol and the second weight loss around 650°C was corresponded to the full destruction of MOF. So to ensure the complete metal reduction, a high temperature of 700°C was chosen for calcination (Fig. S3).

Catalyst characterization. The obtained catalyst was characterized by powder X-ray diffraction (PXRD), Barnauer-Emmett-Teller (BET) nitrogen adsorption, scanning electron microscopy (SEM), electron microprobe analysis (EPMA), energy dispersive X-ray spectrometer (EDS) and Atomic adsorption spectroscopy (AAS).

XRD pattern of fresh catalyst is shown in Fig. 1. The fresh catalyst exhibits diffraction peaks of spinel mixed metal oxides NiCo_2O_4 , Co–Ni alloy and metallic (Co and Ni) phases. X-ray diffractograms showed that the mixed metal oxides crystallized in the spinel phase with space group $Fd\bar{3}m$. As shown in Fig. 1 the diffraction peaks of Co–Ni are located at $2\theta = 16^\circ, 21.5^\circ, 24.4^\circ, 30.6^\circ, 41.3^\circ,$ and 61° . This demonstrates that metal nickel and cobalt reduced in the state of alloy. The characteristic diffraction peaks are weak and broad. The broad and low-intensity identity of these characteristic peaks represents the fine particle size and the high distribution of metal species. Particles size of Co–Ni alloy, single metal and spinel-type oxide are listed in Table 1 according to the Debye-Scherrer equation [14]. The particle size of Co–Ni, single metal phases of Ni, Co and NiCo_2O_4 ranges

from 12 to about 30 nm, indicating that these particles have high specific surface area and good anti-sintering ability. After reaction, the particle size of Co–Ni alloy and single metal phases increased to 22 and ~40–46 nm respectively. It has been reported in the literature that the particle sizes of Co–Ni alloy are smaller than that of single metal particles of Ni and Co, which indicates that the particles of Co–Ni alloy have better anti-sintering ability than that of corresponding single metal particles [15]. These results are consistent with the surface area data, SEM and EMPA results, which showed more porous structure led to high surface area. The high specific surface area allows a high degree of metal dispersion.

From the N_2 adsorption test, the Brunauer-Emmett-Teller (BET) surface area and total pore volume of the catalyst were calculated as $276 \text{ m}^2 \text{ g}^{-1}$ and $0.31 \text{ cm}^3 \text{ g}^{-1}$ respectively. The N_2 adsorption/desorption isotherm of catalyst presented a sharp inflection at a relative pressure in the range of 0.5 (Fig. 2) and exhibit type IV isotherm with hysteresis (type H3) between adsorption and desorption branches, indicating the existence of mesoporous cavities with a very wide size distribution. In such a high pore volume of the catalyst, there is the possibility of more active metals for the desired reaction. Larger pore size of the catalyst (20 nm) can facilitate the diffusion of long-chain hydrocarbon products. These data are consistent with

Table 1. The sizes of particles (nm) derived from PXRD results

Samples	Co–Ni	Ni	Co	NiCo_2O_4
Fresh catalyst	12	25	30	15
Used catalyst	22	40	46	23

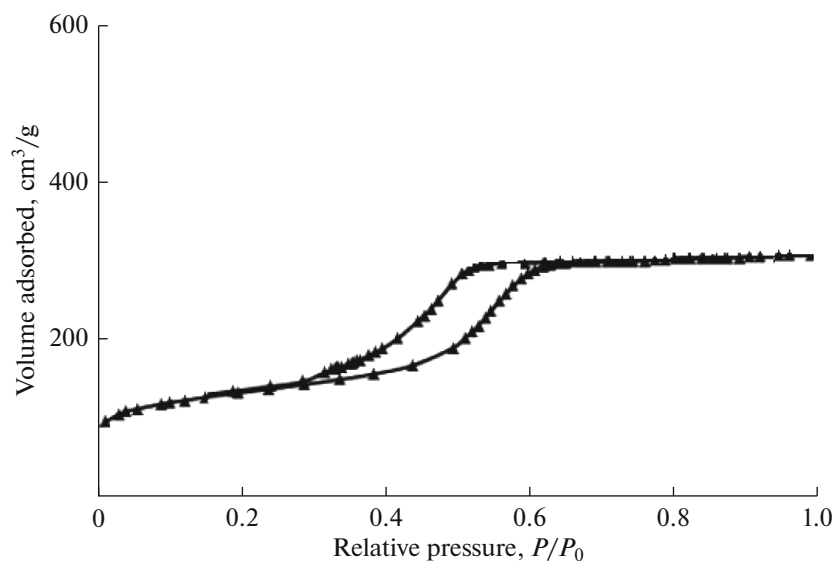


Fig. 2. N₂ adsorption-desorption of the catalyst.

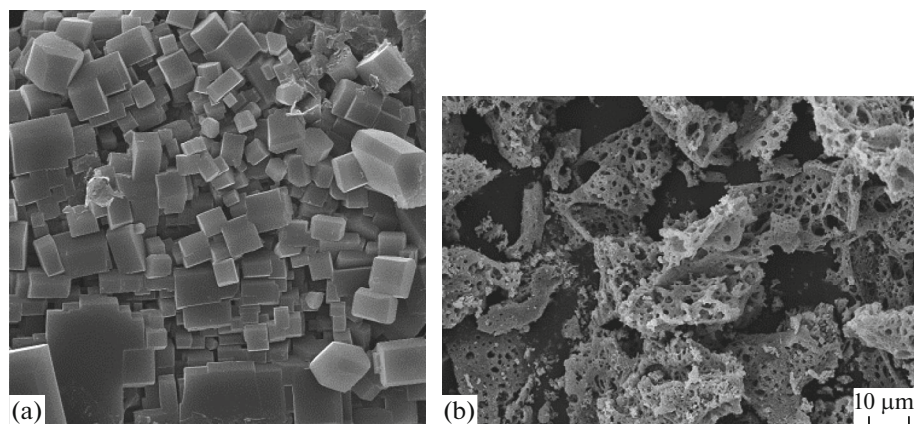


Fig. 3. SEM images of MOF (a) and derived catalyst (b).

the average size acquired from the peak broadening in PXRD studies. Smaller size of the particles leads to higher specific surface area. Furthermore, higher surface area will cause to better distribution of particles. Moreover, wider pore mesoporous is also appropriate to the diffusion of gas, resulting in a higher catalytic activity [10]. These results confirmed by SEM and EPMA studies.

Scanning electron microscopy analysis in combination with elemental mapping (EPMA and EDS) give further information on the morphology of MOF precursor and its corresponding MOF-derived catalyst. It is apparent that MOF precursor has well-defined cubic shape (Fig. 3a). During the calcination, the morphological characteristics of the MOF-derived catalyst are completely different and it was deforming into a highly porous, loose and low density sample (Fig. 3b) that is appropriate for

catalytic applications. Figure 4 shows the EPMA results for the catalyst. The distribution of Co and Ni is entirely homogeneous and it was uniform on an atomic level.

Additional analysis by combining EDS was conducted to analyze the surface elemental composition. The EDS spectrum of the catalyst (Fig. 5) reveals the presence of both Co, Ni, C and N, which is confirmed by powder X-ray diffraction data. The Co and Ni contents in the catalyst were measured by atomic adsorption spectroscopy (AAAnalyst 200, PerkinElmer, USA). These data are consistent with ICP-MS (PerkinElmer's NexION 2000 ICP Mass Spectrometer) results (22.38% Co and 21.97% Ni). Results showed the high metal loading and superb dispersion of Co and Ni (44.35%) at the surface of the catalyst. The elemental composition characterization of the catalyst showed presence of nitrogen, oxygen and car-

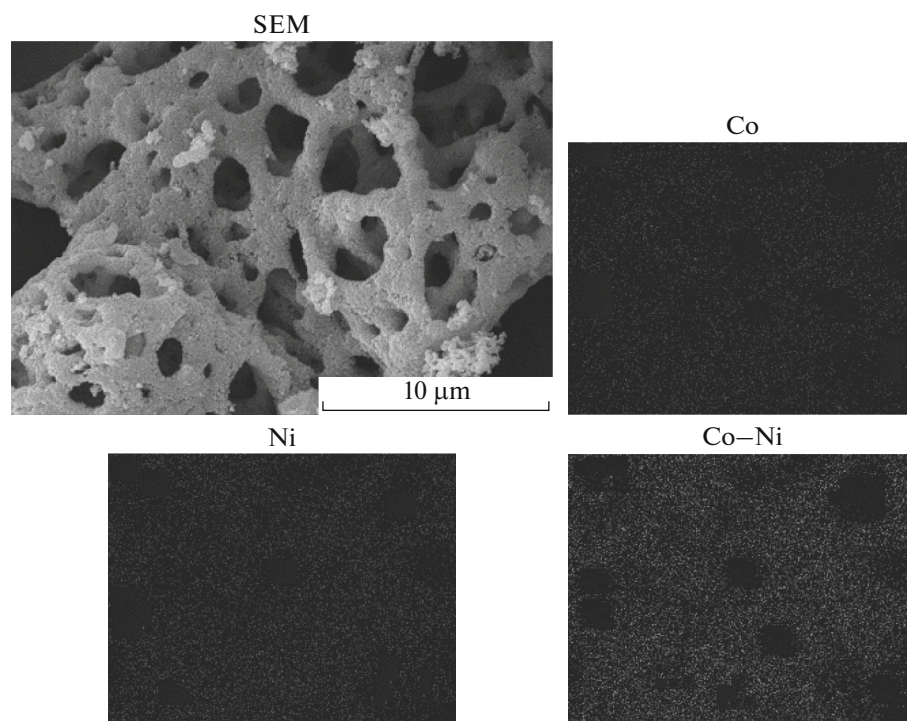


Fig. 4. Elemental mapping (EPMA) of the catalyst.

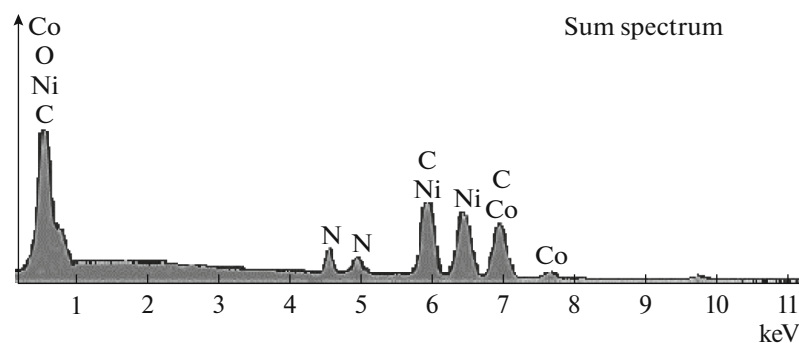


Fig. 5. EDX spectrum of the catalyst.

bon in the derived catalyst (C 45.18%, O 5.41% and N 5.06%).

Catalytic performance results. The MOF-derived catalyst was tested in FTS reaction under 1 MPa pressure and $H_2/CO = 2$. The product distribution and catalytic activity are presented in Table 2. The activity of the catalyst was tested between 260–340°C. It should be noted that CO conversion was low at temperatures below 260°C (~40%). The CO conversion was increased almost linearly with increasing temperature reaction. Obviously, the reaction rate increases at high temperatures. Due to the increase in the number of effective collisions, the reaction conditions are more suitable and the faster the reaction rate. At 320°C the CO conversion increased to 75%, which

showed that desired catalyst exhibited high FT activity compared with most reports in the literature [2, 9, 10, 16]. The notable CO conversion of the catalyst should be attributed to high surface area (according to BET measurements), high metal loading percentage (based on elemental analysis and EPMA results) and porous texture of the catalyst (confirmed by SEM results). Furthermore, larger pore size of the catalyst can facilitate the diffusion of gas in the carbon matrix therefore, enhanced the catalytic activity (based on N_2 sorption test). The product selectivity of the catalyst is also perceptible against other MOF-derived cobalt catalysts. Since in Fischer-Tropsch reaction, CO converts to CO_2 and hydrocarbon products (C_1-C_n) and because C_5^+ products are volatile liquid, they often

Table 2. Catalytic performance of the MOF-derived catalyst in FT synthesis

Temperature, °C	CO conv., %	Hydrocarbon selectivity, %				TOF, s ⁻¹
		C ₂ –C ₄	C ₅ ⁺	CH ₄	CO ₂ selectivity, %	
260	48	26.0	39.6	14.0	9.8	1.33
280	51	27.5	46.0	14.8	6.4	1.41
300	63	28.1	48.4	15.2	4.1	1.75
320	75	30.3	51.8	15.7	1.2	2.08
340	75	30.8	51.9	16.6	0.4	2.08

Total sum of the selectivity values is less than 100%. It can be attributed precisely to the loss of the volatile part of C₅⁺ hypothetically and its value systematically increases with decreasing temperature.

remain in the path of the reactor and are not detected by GC. The selectivity of C₅⁺ products reached 52% and the selectivity towards short-chain olefins (C₂–C₄) were 30.3% (at 320°C). It is obvious that Co–Ni based FTS catalysts commonly have higher selectivity towards long-chain hydrocarbons. These catalytic performance results are much higher than the most FTS catalysts reported in the literature [2, 9, 10, 16–18]. It was reported in the literature that nitrogen species are prominent components in the catalyst framework. In fact, N species are considered as impressive electron donor for increasing the CO adsorption-dissociation process and selectivity of final products in Fischer–Tropsch synthesis. The presence of nitrogen species as effective electron donor, enhanced the CO adsorption-dissociation, varied cobalt valance state and thus, enhanced the synthesis of the short-chain hydrocarbon products. This strong electrostatic interaction has significant impact on the physicochemical properties of cobalt particles especially in the reduction behavior. The electrostatic interaction of cobalt oxide and nitrogen can cause that the reduction of oxides proceeds by releasing the oxygen atoms from the lattice and the free particles would be easily reduced. Similar results were obtained by the other reports [9, 10, 19–22].

The stability of the catalyst was investigated by running the reaction for 200 h at 320°C, 1 MPa, H₂/CO = 2 and GHSV of 3600 h⁻¹. There was no evidence of catalyst deactivation at 200 h. The activity of the catalyst and selectivity towards hydrocarbons did not undergo considerable changes during the test. Supreme stability of the catalyst is also affected by its texture structure. Based on N₂ sorption test, the pore size of the catalyst is large. Wide pore mesoporous in addition to increasing catalytic activity, because of the facilitated diffusion of gas into the carbon matrix, causes deactivation of the catalyst to be postponed. Conversely, in tight pore catalysts by forming hydrocarbons, the active sites covered by products and thus the catalyst was deactivated. Along with the formation of active phases, the notable performance of this MOF-derived catalyst should be related to its high loading percentage, abundant porosity and high pore volume of the catalyst. Catalysts with these properties can be served as ideal catalysts for Fischer–Tropsch process. As the

results shown, the catalytic performance is related to physicochemical characteristics of the catalyst. The catalytic properties are often affected by two factors: the preparation procedure and the nature of the precursor. Above mentioned results highlighted the importance of the preparation route onto catalytic properties and FTS efficiency. We compared this catalyst with a variety of mono and heterobimetallic cobalt-based catalysts prepared via different preparation procedures. Many of the characteristics and performances of this catalyst are comparable to previous reports and according to the catalyst novelty, it has notable performance. For example, catalyst stability was higher (200 h of work without significant changes of the catalyst performance) than 102 h [2] and 50 h [23]. In comparison with the other cobalt-based catalyst reported in literature [2, 8, 17, 18], this catalyst showed good selectivity towards short-chain hydrocarbons (selectivity to C₂–C₄ products of 30% compared with 6 [2], 14 [8], 22 [17], and 11% [18]). The catalyst also had a relatively high selectivity to C₅⁺ products of ~52% compared to the other Co-based catalysts, which are reported in literature: 10 [8], 54 [17], and 49.83% [18]. Turnover frequency (TOF) for the presented catalyst were calculated (Table 2) and comparable to (or greater) those measured on typical MOF-derived catalysts (TOF of 0.0019, 0.031, 0.028 s⁻¹ [2], 0.027, 0.091 s⁻¹ [9], and 0.07, 0.11 s⁻¹ [16]). The CO conversion in this catalyst (75%) is also high compared to the reported values: 15.8 [2], 30 [10], 44.5 [8], 16 [17], and 37.34% [18]. Above mentioned results demonstrate that this new catalyst is very promising in FTS against other MOF-derived cobalt catalysts.

CONCLUSIONS

In the present study, a heteronuclear Co–Ni complex was used as a metal-organic framework for preparation of an active Co–Ni FTS catalyst. MOF-derived FT catalyst prepared via glycine–MOF combustion method. It was utilized as an unsupported catalyst without any promoter, which resulted a high metal content (44.35 wt %) in the catalyst. By using this method, highly loaded metal nanoparticles (22.38 wt % Co, 21.97 wt % Ni) with well dispersion

was obtained. Characterization and catalytic performance results demonstrate that desired catalyst showed notable activity (TOF of 2.08 s^{-1}) and good selectivity to C_5^+ products (52%). The results here presented indicate that the glycine–MOF combustion synthesis strategy is an approving route for the preparation of especially dispersed metal nanoparticles in a porous matrix with prominent FTS performance. To the best of our knowledge, this unsupported MOF-catalyst is one of the active and stable FT catalysts. Its notable performance can be ascribed to the enhanced active surface areas of well-dispersed nanoparticles, porous structure and high pore volume of the derived catalyst. We discovered that mentioned synthesis strategy resulted in favorable properties such as porous structure, high loaded, stable and active metal catalysts, which it has never been reported before so it can be coping with a serious challenge in industrial catalysts.

FUNDING

Funding of this work by the University of Sistan and Baluchestan is gratefully acknowledged.

CONFLICT OF INTEREST

Authors declare that they have no conflict of interest.

SUPPLEMENTARY MATERIALS

Supplementary information for this paper is available for authorized users at <https://doi.org/10.1134/S0965544120090121>.

THE AUTHORS ORCID ID

Halimeh Janani, ORCID: <http://orcid.org/0000-0003-2750-7074>

Alireza Rezvani, ORCID: <http://orcid.org/0000-0003-2681-9906>

Ali Akbar Mirzaei, ORCID: <http://orcid.org/0000-0002-1753-2340>

REFERENCES

1. L. Jiao, Y. Wang, H. L. Jiang, and Q. Xu, *Adv. Mater.* **30**, 37 (2018).
2. X. Sun, A. I. O. Suarez, M. Meijerink, et al., *Nat. Commun.* **8**, 1680 (2017).
3. Y. Cui, B. Li, H. He, et al., *Acc. Chem. Res.* **49**, 483 (2016).
4. M. B. Majewski, A. W. Peters, M. R. Wasielewski, et al., *ACS Energy Lett.* **3**, 598 (2018).
5. L. C. Almeida, F. J. Echave, O. Sanz, et al., *Chem. Eng. J.* **167**, 536 (2011).
6. A. N. Pour, M. R. Housaindokht, J. Zarkesh, and S. F. Tayyari, *J. Ind. Eng. Chem.* **16**, 1025 (2010).
7. X. Yan, Q. Huang, B. Li, et al., *J. Ind. Eng. Chem.* **19**, 561 (2013).
8. H. Janani, A. R. Rezvani, G. H. Grivani, and A. A. Mirzaei, *J. Inorg. Organomet. Polym. Mater.* **25**, 1169 (2015).
9. B. An, K. Cheng, C. Wang, et al., *ACS Catal.* **6**, 3610 (2016).
10. B. Qiu, C. Yang, W. Guo, et al., *J. Mater. Chem. A.* **5**, 8081 (2017).
11. Y. Wang, J. Zhu, L. Zhang, et al., *Mater. Lett.* **60**, 1767 (2006).
12. M. A. Vannice and R. L. Garten, *J. Catal.* **66**, 242 (1980).
13. S. Zhang, Q. Xing, and W. H. Sun, *RSC Adv.* **6**, 72170 (2016).
14. P. Ciambelli, S. Cimino, S. De Rossi, et al., *Appl. Catal., B.* **24**, 243 (2000).
15. Z. Wang, C. Wang, S. Chen, and Y. Liu, *Int. J. Hydrogen Energy* **39**, 5644 (2014).
16. V. P. Santos, T. A. Wezendonk, J. J. D. Jaén, et al., *Nat. Commun.* **6**, 6451 (2015).
17. J. Ye, S. Haiquan, B. Fenghua, et al., *Appl. Organometal. Chem.* **23**, 86 (2009).
18. Z. Shanghong, D. Dongping, B. Fenghua, and S. Haiquan, *J. Rare Earth.* **29**, 349 (2011).
19. T. Fu, R. Liu, J. Lv, and Z. Li, *Fuel Process. Technol.* **122**, 49 (2014).
20. L. He, F. Weniger, H. Neumann, and M. Beller, *Angew. Chem. Int. Ed.* **55**, 12582 (2016).
21. Z. Yang, S. Guo, X. Pan, et al., *Energy Environ. Sci.* **4**, 4500 (2011).
22. Y. F. Yang, L. T. Jia, B. Hou, et al., *J. Phys. Chem. C* **118**, 268 (2014).
23. H. J. Schulte, B. Graf, W. Xia, and M. Muhler, *Chem. Cat. Chem.* **4**, 350 (2012).